GEOPHYSICAL CHARACTERISTICS OF VON KÁRMÁN CRATER: CHANG'E 4 LANDING SITE REGION. Gregory A. Neumann[1*], James W. Head[2], [1]NASA Goddard Space Flight Center, Greenbelt, MD 20771 (gregory.a.neumann@gmail.com), [2]Department of Earth, Environmental and Planetary Sciences, Brown University, Providence RI 02912.

Introduction: The lunar farside South Pole-Aitken (SPA) basin is an area of low elevation (~6 km below the reference sphere), thin (~17 km average) crust, in which are situated the Von Kármán impact craters [1, 2]. Von Karman crater (186 km) lies within the Mg-Pyroxene Annulus of the SPA basin [3]. The Pre-Nectarian crater has been flooded by mare basalts during the Imbrian Period, but a portion of its central peak remains exposed at the crater center (Fig. 1a) [e.g., 4-6]. On 3 January 2019, the Chinese Lunar Exploration Program successfully landed the Chang'E 4 lander on the farside of the Moon, on the southern floor of the Von Karman crater [1]. *In situ* exploration within the Von Karman landing region will bring unprecedented spectral, radar, and imaging data for the landing area, improving our understanding of the farside mare basalts, SPA compositional zones (such as the Mg-Pyroxene Annulus), regolith evolution, and the space environment [1]. Understanding the geophysical characteristics of the landing site, as we analyze here, is complementary to these objectives and provides a broad context.

High-resolution gravity data from the Gravity Recovery and Interior Laboratory (GRAIL) mission and topography from the Lunar Orbiter Laser Altimeter (LOLA) [7-8] analyzed here provide improved resolution of the crustal structure at the Chang'E 4 landing site (~45.5°S 177.6°E), revealing two basin-like circular regions of uplifted mantle resulting from two ancient impacts (Fig. 1), and a highly variable crustal thickness (0-30 km). The reported lander location lies on the thicker annulus of crust between the uplifted mantle plugs, and is situated on ~15-km-thick crust with a steeply sloping crust-mantle interface.

Regional spectral analyses of gravity/topography correlations in 7.5°–15° wide windows [9-10] suggest lateral and vertical variations in crustal density. These models have a shallow low-density (porous) surface layer (< ~2200 kg m^{-3}), with a significantly thinner low-density layer than the rest of the lunar farside, with crustal density increasing rapidly with depth within the uppermost 5 km. We study the correlation of gravity with topography in two smaller (4°x3.5°) regions where unmodified craters probe the upper 3-4 km of target material to study the geophysical characteristics of the Chang'E 4 landing site region.

Methods: We first analyze the gravity anomaly [10] using a density reduction of 2550 kg m^{-3} and downward-continue the resulting Bouguer gravity potential disturbance (Fig. 1b) to a crust-mantle density interface, globally constrained by the Apollo 12-14 seismic experiment results [11]. Previous work minimized the geological "noise" effect of intracrustal density heterogeneities [12] by means of a minimum-structure filter [13] which effectively limited spatial resolution to spherical harmonic degree 80-90, depending on depth. For this study we relax the filter constraint to ~170 degree and order half-power [7], and obtain nearly twice the spatial resolution, at the expense of increased complexity.

The correction of the gravity field for surface topography is performed using a uniform density but Fig. 1b shows several craters for which that density does not fully account for the mass deficit of the excavated volume relative to the target surface. We varied the density to minimize via least-squares the residual Bouguer disturbance over regions roughly twice the area of the crater. These well-preserved impacts [14] allow a detailed estimation of the density of the target material that was excavated. Smaller contributions from impact melt ponds, fractured/comminuted floor material [15] or possible volcanic intrusion may affect the estimate, but these effects are secondary to that of the excavated crater topography itself.

Results: A previous crustal thickness model is shown in Fig. 1c, including thickness variations due to surface topography, and a higher-resolution model of the mantle relief in Fig. 1d. The models show steep lateral gradients in crustal thickness and two local regions of uplifted mantle associated with the central peaks of the craters. Quantitative thicknesses must be confirmed by other techniques but the overall 30 km variation is a robust result.

The very thin local crust shown in the higher-resolution model (Fig. 2) suggests that the Chang'E 4 rover may have the opportunity to explore mantle-derived mineralogy if any superposing impacts excavated these materials. These materials could be derived from a central peak or peak-ring formation in Von Kármán M that was later exposed along the Von Kármán impact rim.

Crustal density: The 3.9-km-deep Finsen crater lies immediately northeast of the Chang'E 4 site and its ejecta and secondaries cover the region [1]. Finsen is one of three well-preserved complex craters chosen to establish depth-diameter relationships in SPA [14]. We find a best-fitting target material density of 2770±50 kg m^{-3}, substantially higher than the surface density inferred from spectral analysis within SPA [9-10]. Simi-

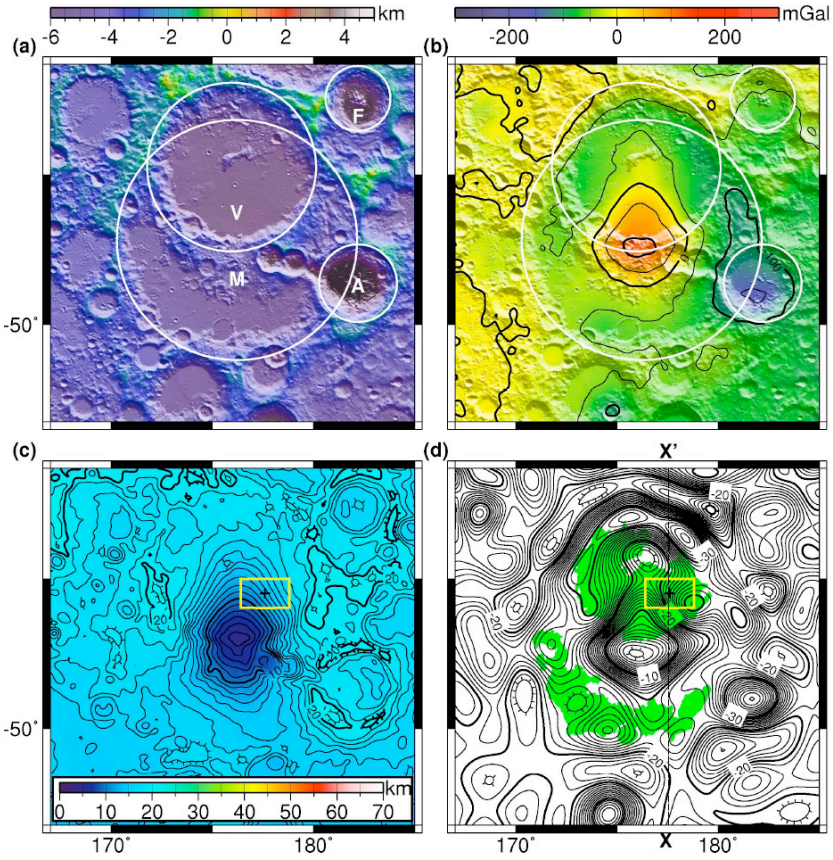

Fig. 1. (a) Topography of SPA region in Mercator projection. Circles outline the rims of the Von Kármán (V) crater (219 km diameter) and Von Kármán M basin (M) (245 km diameter), as well as the deep and relatively fresh Finsen (F) and Alder (A) craters. **(b)** Bouguer gravity anomaly (50 mGal contours) bandpassed from spherical harmonic degrees 6 to 660. **(c)** Crustal thickness model [7] filtered to ~65 km spatial resolution (1 km contours). The targeted lander location is outlined in yellow. **(d)** Crust-mantle interface height relative to a 1738-km-radius sphere, from higher-resolution downward continuation. Tickmarks denote locally high relief. Regions mapped as mare are shown in green. Profile X-X' is illustrated in Fig. 2.

larly, the Alder crater has a density of 2950±50 kg m^{-3}. Such densities indicate relatively low porosity and/or high mineral grain density [16].

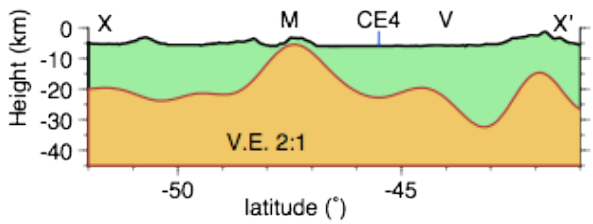

Fig. 2. Profile S-N through the Chang'E 4 landing site. Depth to crust-mantle interface (brown) shows asymmetric central uplift beneath the Von Kármán crater, and a thickened crustal collar beneath the targeted site.

Discussion: The Von Kármán M basin is smaller than the well-preserved Poincaré and Planck peak-ring basins within SPA, but is larger than two peak-ring basins (Schwarzchild, d'Alembert) in the lunar highlands [17-18]. While it lacks a peak ring, it is possible that its morphology has been erased by later impacts and volcanism, or that there is an influence of crustal thickness on the size of peak-ring basin onset [19] with the strength profile of thinner target crust resulting in no lasting peak rings in model simulations. The immediately adjacent, similarly sized, well-preserved Leibnitz crater also lacks a peak ring. Regional magnetic anomalies [20] and the broader geologic context [21] are also of interest.

Conclusions: The very thin crust in the immediate vicinity of the Chang'E 4 lander, as well as the steep gradients in mantle relief, are likely to produce a variety of compositions when excavated by nearby impacts, providing new windows into the lunar farside.

References: [1] Huang J. et al. (2018) JGR, 123, 1-17. [2] Neumann G A et al (2015) Science Advances, 1(9), e1500852. [3] Moriarity D. and Pieters C. (2018) JGR Planets, 123, 729-747. [4] Losiak A. et al. (2009) LPSC #1532. [5] Yingst R, et al. (2017) LPSC #1680. [6] Pasckeret J. H. et al. (2018) Icarus, 299, 538-562. [7] Zuber M. T. et al. (2016) Science, 354(6311), 438–441. [8] Smith D.E. et al. (2017) Icarus, 283, 70–91. [9] Besserer J. et al. (2014) GRL, 41, doi:10.1002/2014GL060240. [10] Goossens S. J. et al. (2018) AGUFM. [11] Wieczorek M. A.. et al. (2013) Science, 339, 671–675. [12] Jansen J. C. et al. (2017) Icarus, 291, 107-123. [13] Wieczorek M. A. & Phillips R. J. (1998) JGR: Planets, 103(E1), 1715-1724. [14] Kalynn, J. et al. (2013) GRL, 40(1), 38-42. [15] Soderblom, J. M. et al. (2015) GRL 42(17) 6939-6944. [16] Kiefer W. S. et al. (2012) GRL, 39(7). [17] Baker D. M. et al. (2016) Icarus, 273, 146-163. [18] Baker D. M. et al. (2017) Icarus 292, 54-73. [19] Johnson B. C. et al. (2018) JGR: Planets, 123(11), 3035-3050. [20] Ravat et al. (2019) LPSC 50. [21] Ivanov, M. A. et al. (2018) JGR Planets, 123, 1-28.